Science Advances
AAAS

Supplementary Materials for

Flaw-insensitive fatigue resistance of chemically fixed collagenous soft tissues

Liangsong Zeng *et al.*

Corresponding author: Jingda Tang, tangjd@mail.xjtu.edu.cn; Zhigang Suo, suo@seas.harvard.edu

Sci. Adv. **9**, eade7375 (2023)
DOI: 10.1126/sciadv.ade7375

This PDF file includes:

Table. S1 Fracture toughness of soft tissues.

Tissue	Fracture toughness (kJ/m^2)	Ref
Rat skin	12 (P), 24 (N)	(*27*)
Sea anemone mesoglea	1.21	(*27*)
Porcine aorta	1~2.5 (P)	(*28*, *29*)
Bovine muscle	0.42 (P), 1.83 (N)	(*30*)
Rhinoceros dermal	77.6 (Superficial), 43.0 (Deep)	(*31*)
Articular cartilage	0.14~1.2 (P)	(*32-34*)
Human skin	1.7~2.6	(*35*)
Liver tissues	0.2	(*36*, *37*)
Porcine skin	4.1 (adipose),17 (dermal)	(*38*)
Porcine muscle	2.49 (P)	(*39*)
Bovine pericardium	32~35	(*40*, *41*)
Bovine Glisson's capsule	4.5	(*42*)

*Footnotes: (P) Precut is parallel to the fiber direction. (N) Precut is normal to the fiber direction.

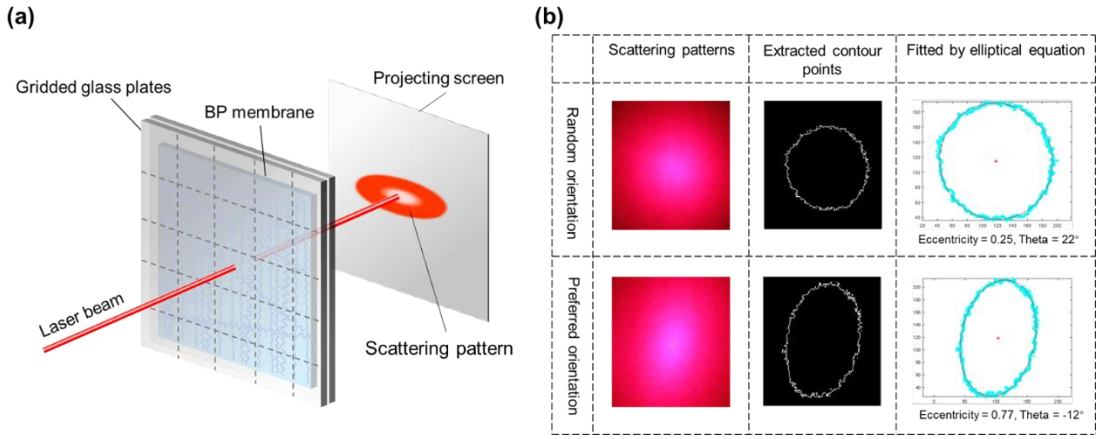

Fig. S1. Detecting orientation of collagen fibers in bovine pericardium (BP) membrane through small-angle light scattering (SALS). (a) Schematics of SALS. After the laser beam perpendicularly passes the BP membrane, a scattering pattern is projected on the screen. (b) A circular scattering pattern indicates a random orientation of collagen fibers, and an elliptical scattering pattern indicates a preferred orientation of collagen fibers. By fitting the extracted contour of a scattering pattern to the equation of an ellipse, we determine the degree and the direction of alignment of collagen fibers.

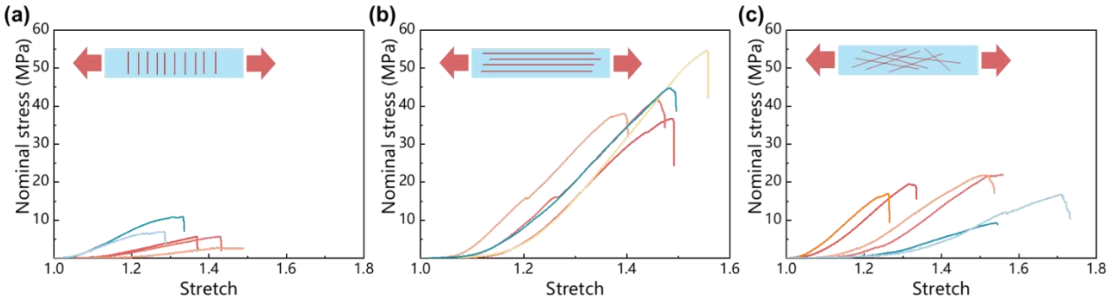

Fig. S2. Stress-stretch curves of BP samples in different groups. (a) Stretch in the direction normal to the orientation of collagen fibers. (b) Stretch in the direction parallel to the orientation of collagen fibers. (c) Stretch of samples in which collagen fibers are randomly oriented in the undeformed state.

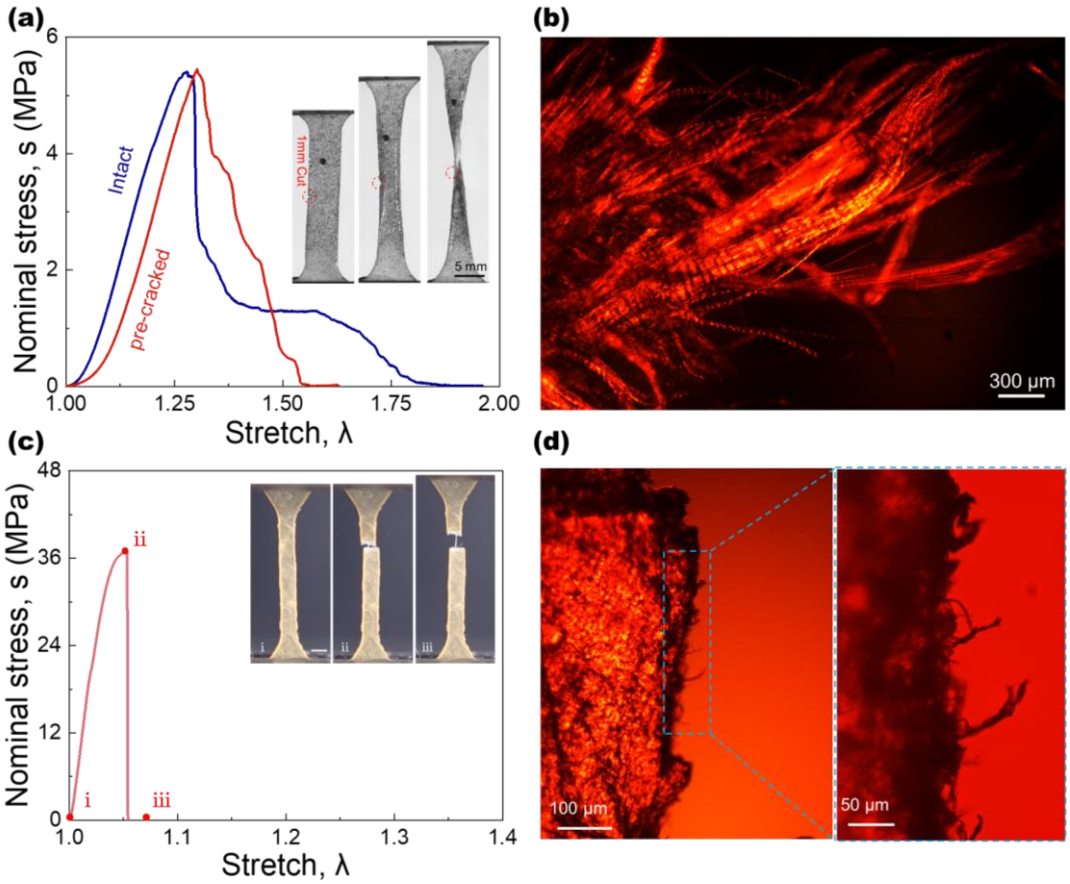

Fig. S3 Tension of pre-cracked sample and dehydrated sample. (a) Stress-stretch curves of samples with and without precut, along with snapshots of single-edge cracked sample at different stages of deformations. (b) Polarized-light micrograph of rupture surface from pre-cracked sample. (c) Stress-stretch curve of dehydrated sample, along with snapshots of three states of deformation. (d) Polarized light micrograph of the rupture surface. At the rupture surface, the pullout length of collagen fibers is ~50 μm. The mass of the dehydrated sample is 28% of the original sample.

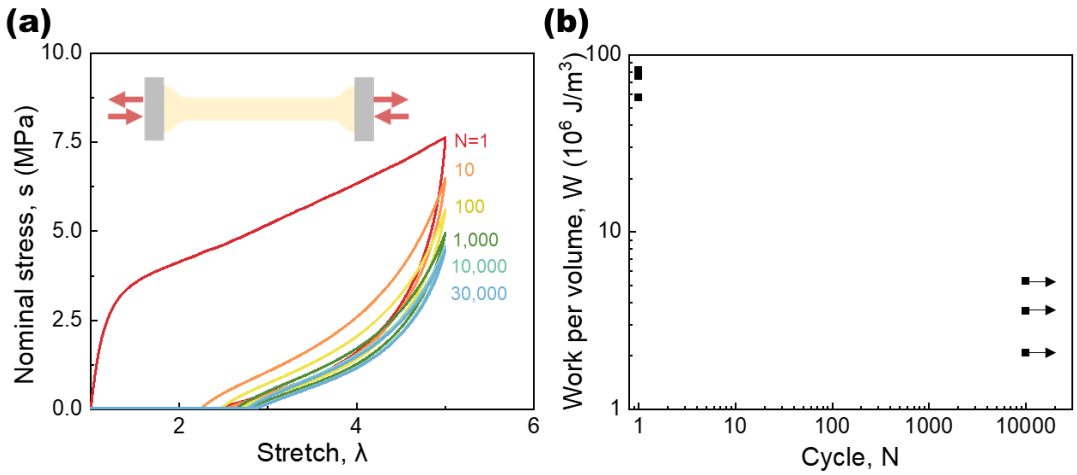

Fig. S4 Fatigue test of thermoplastic polyurethane (TPU) samples without precut. (a) Stress-stretch curves under cyclic stretch. (b) The number of cycles to rupture is a function of the amplitude of work per volume. The amplitude of work per volume is between two limits: the work of fracture W_c, at which the sample ruptures under monotonic stretch; and the work of endurance W_e, at which the sample survives a prescribed number of cycles of stretch. For the TPU, $W_c \sim 100\times10^6$ J/m^3 and $W_e \sim 10\times10^6$ J/m^3.

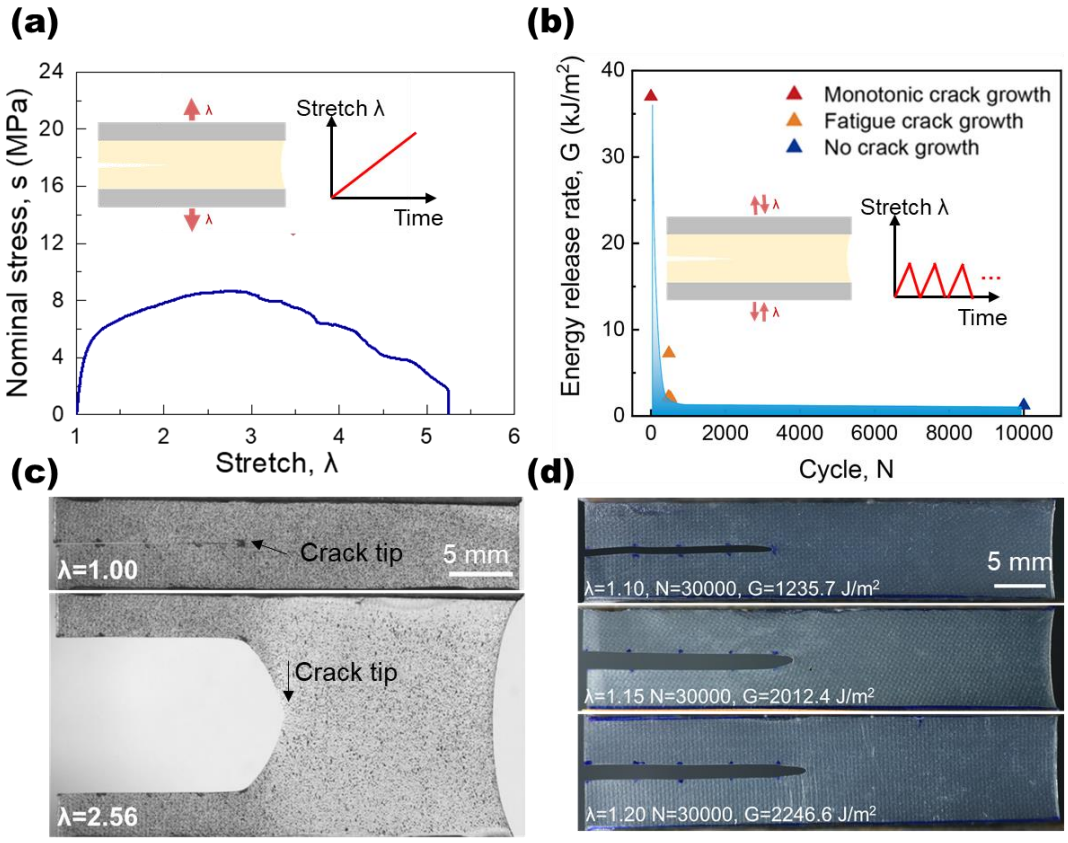

Fig. S5 Crack growth in TPU membranes under monotonic and cyclic stretch. (a) Stress-stretch curve under monotonic stretch. (b) The number of cycles to fail as a function of the amplitude of energy release rate. The amplitude of energy release rate is between two limits: the fracture toughness G_c, at which the sample grows crack under monotonic stretch; and the threshold of energy release rate G_{th}, under which the sample survives a prescribed number of cycles of stretch. For the TPU, $G_c \sim 40$ kJ/m^2 and $G_{th} \sim 1.2$ kJ/m^2. (c) Photos of a sample before and after a monotonic stretch. Marked in each photo is the position of the crack tip. (d) Photos of samples after 30,000 cycles of loading at several amplitudes of stretch and energy release rate. The crack does not grow in the sample under $G = 1235.7$ J/m^2, but grows in the samples under $G = 2012.4$ J/m^2 and $G = 2246.6$ J/m^2.

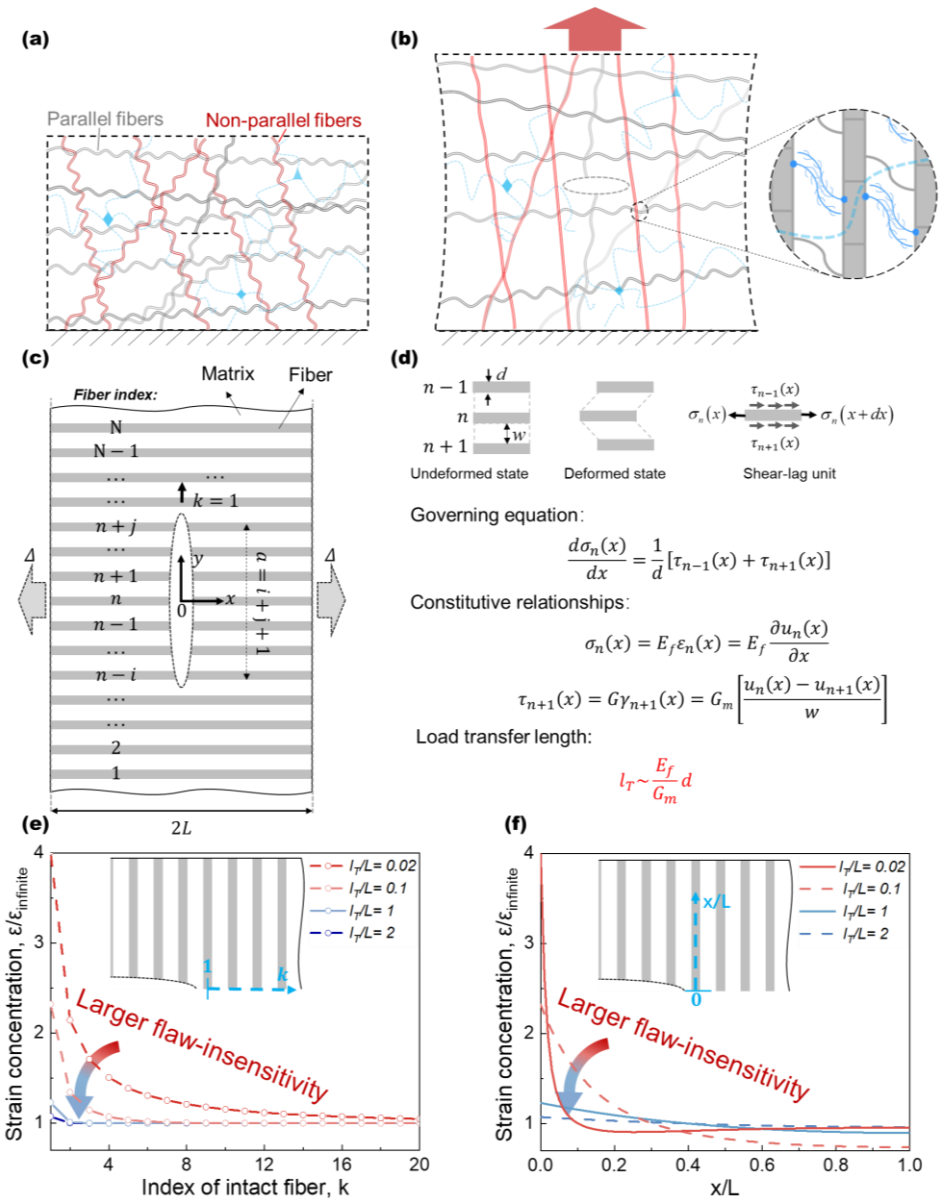

Fig. S6 Discrete model for the flaw-insensitivity of BP. (a) BP membrane with a flaw in the undeformed state. (b) BP membrane with a flaw in the deformed state. Non-parallel collagen fibers (in red color) will reorient to the direction of applied stretch and bear tension. (c) The BP membrane is simplified into a pre-cracked fiber reinforced composite. Only those collagen fibers in the direction of force are modelled as load bearing fibers. The rest part is defined as inter-fiber matrix with low shear modulus. (d) Separated body unit and governing equations. The load transfer length, l_T, measures the flaw-insensitivity of a material. $l_T \sim dE_f/G_m$ =1.5 cm for the BP membrane. d is obtained from the SEM images in Fig. 3c. Given the crack size a, and the sample size L, we show how the strain concentration in intact fibers ahead the crack tip is affected by the flaw-insensitivity of materials. The strain concentration is defined by normalizing the local strain ε by the far-field strain $\varepsilon_{infinite}=\Delta/L$. (e) The strain concentration in a bundle of intact fibers ($x=0$) ahead of the crack tip. (f) The strain concentration in the first intact fiber ($k=1$) ahead of the crack tip. Red lines indicate the tension in an intact fiber is limited in a short length at the crack tip when the materials are sensitive to the crack. The strain field is determined by numerically solving a group of ODEs through MATLAB.

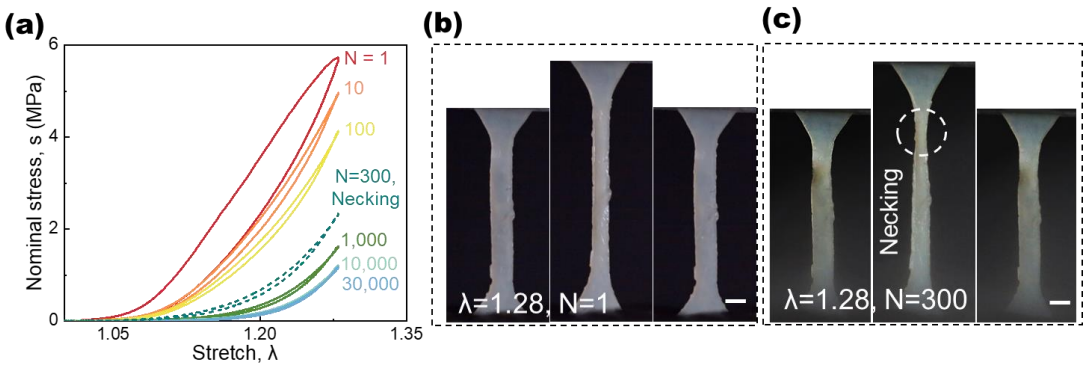

Fig. S7 Necking of BP samples in fatigue test. (a) Stress-stretch curve. Snapshots of samples before (b), and (c) after necking appears.

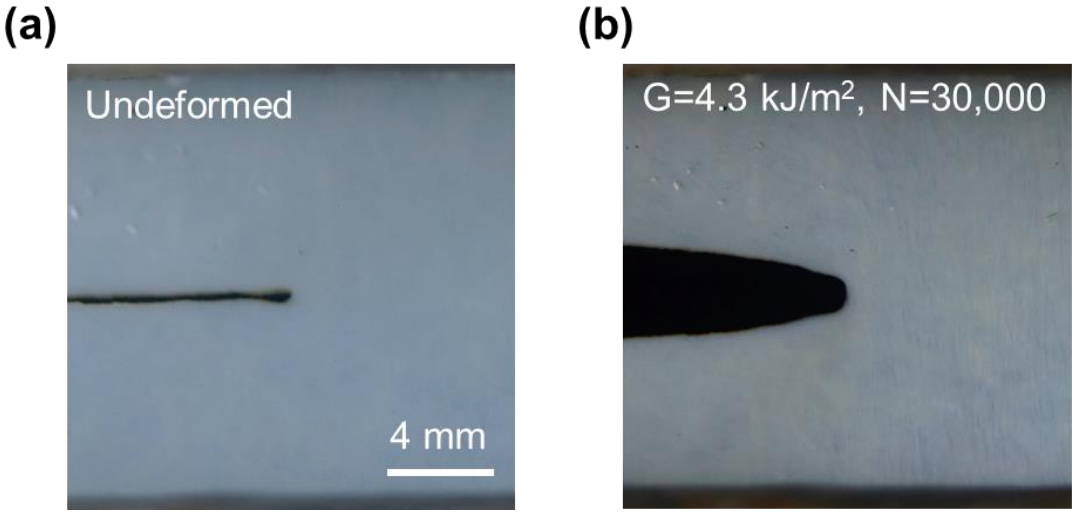

Fig. S8 A crack does not grow in a BP membrane under cyclic loading of a low amplitude of energy release rate. (a) Photo of the sample in the undeformed state. (b) Photo of the sample after 30,000 cycles of stretches, with the amplitude of energy release rate ~4.3 kJ/m^2. No bridging zone is observed at the cut tip after 30,000 cycles.

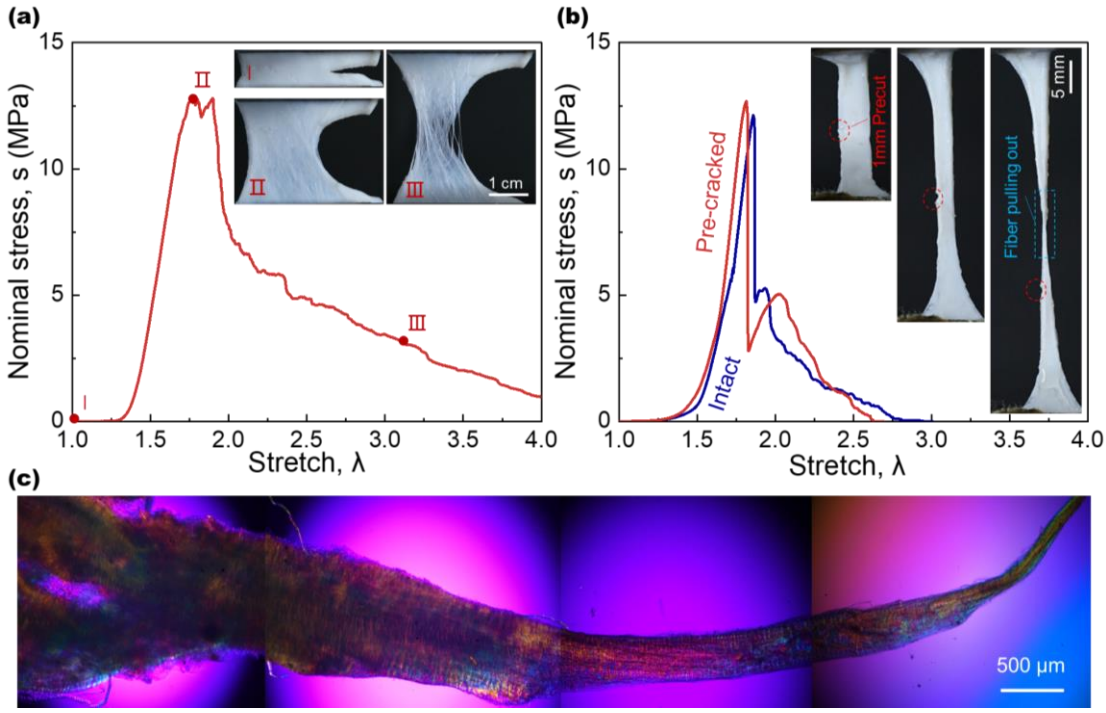

Fig. S9 Fracture and flaw-insensitivity of fresh BP. (a) The stress-stretch curve is recorded in the fracture test, along with snapshots at different stages of deformation. The energy release rate corresponding to stage II is ~22.4 kJ/m^2, taken as the fracture toughness of fresh membrane. (b) Stress-stretch curves of dog-bone shaped samples with and without precuts. The insets show snapshots of the sample with 1 mm precut at different stages of deformation. (c) Polarized light micrograph of rupture surface from the pre-cracked sample. The pullout length of collagen fibers at the rupture surface is ~1cm, longer than that of a chemically fixed membrane.

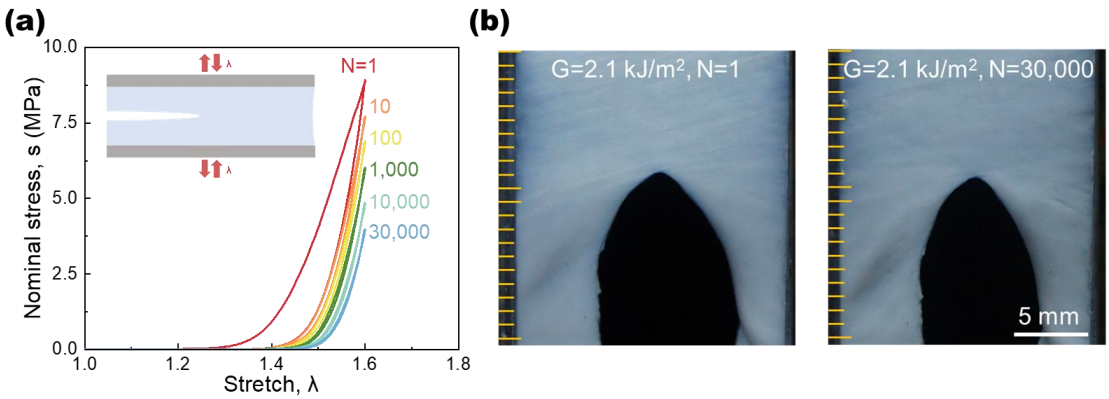

Fig. S10 Flaw-insensitive fatigue resistance of fresh BP. (a) Stress-stretch curves under cyclic stretch. The amplitude of stretch is fixed at 1.60, close to the rupture stretch of intact samples, λ_c=1.70. (b) Photographs of the precut sample before and after 30,000 cycles. No fatigue crack growth can be observed. A sample with a 1.5 cm long precut does not propagate fatigue crack under a stretch close to λ_c, demonstrating that the membrane is insensitive to the precut longer than 1 cm under cyclic stretch.

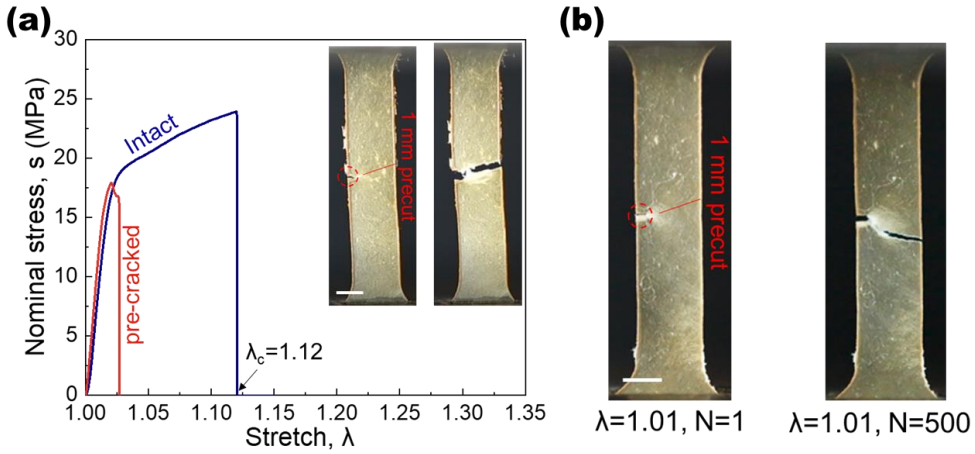

Fig. S11 Reduced flaw-insensitivity of dehydrated BP membrane under monotonic and cyclic stretch. (a) Stress-stretch curves of dehydrated sample with and without precut, along with snapshots showing crack propagation on the pre-cracked sample. (b) Under a small amplitude of cyclic stretch λ=1.01, the 1 mm long precut propagates across the sample after only 500 cycles. Scale bars in (a) and (b) are 2mm.

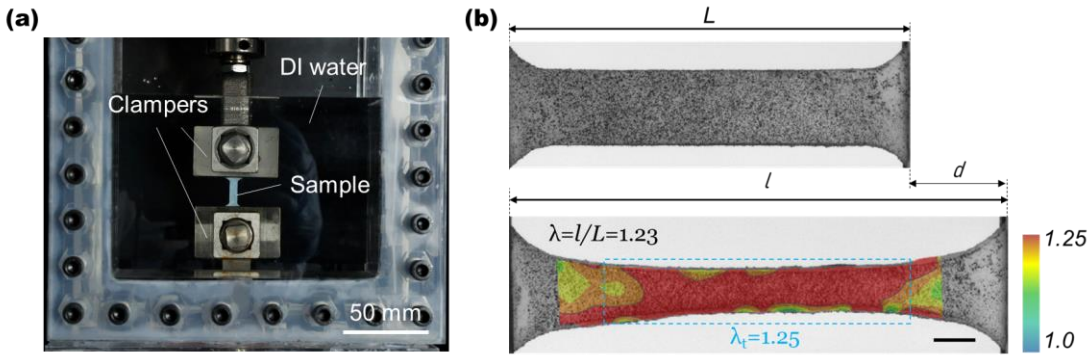

Fig. S12 Experimental method of fatigue test. (a) Photograph of experimental setup. (b) Digital image correlation for calibrating the stretch λ_t in central region by the displacement of clampers *d*. Scale bar in (b) is 2 mm.

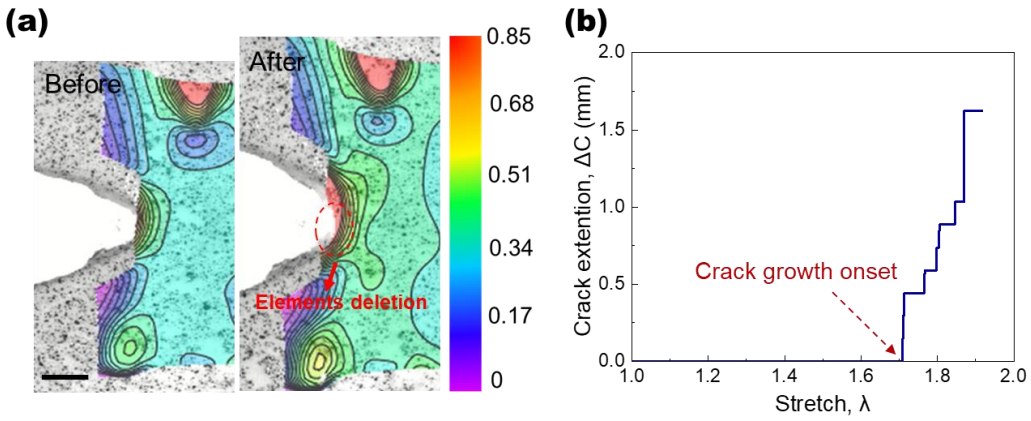

Fig. S13 Measure the crack growth of the membrane through digital image correlation (DIC). (a) DIC images of the membrane before and after the onset of crack growth. Upon crack growth, elements penetrated by separated crack surfaces will be deleted. (b) The crack extension in the undeformed state is determined by counting deleted elements. Scale bar in (a) is 1 mm.

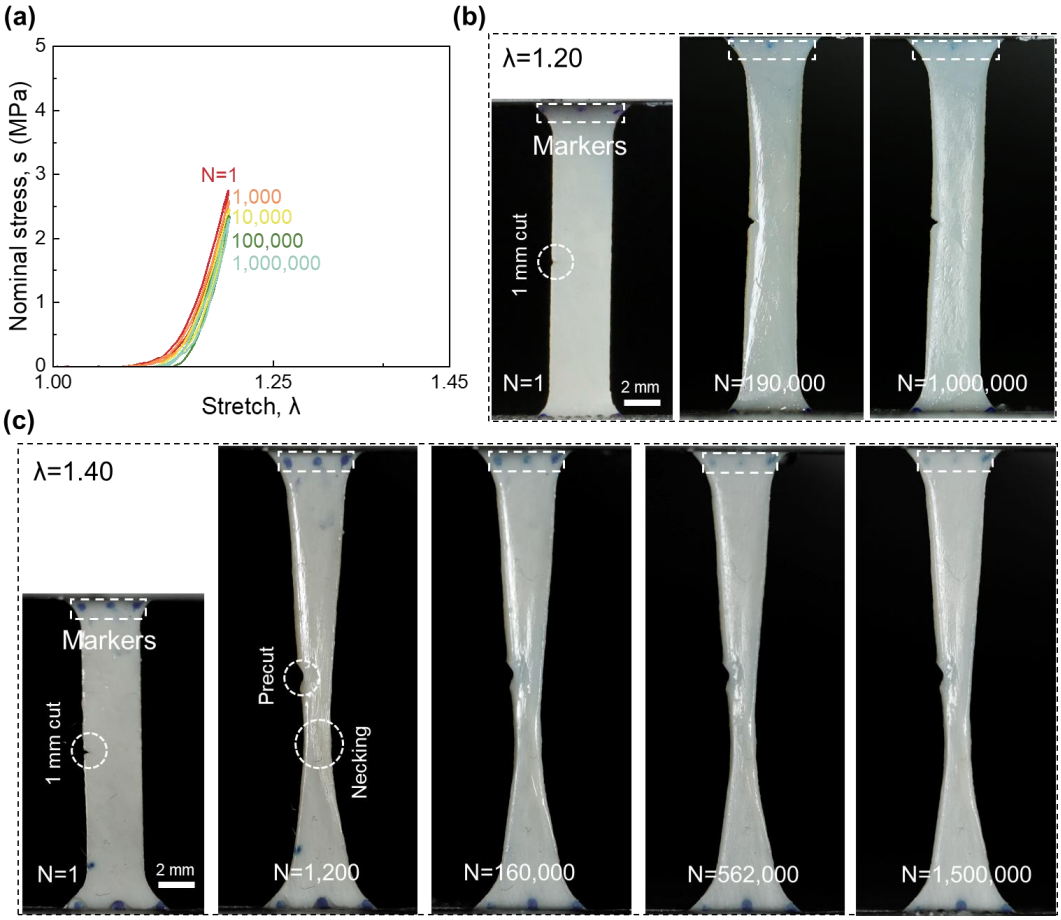

Fig. S14 Fatigue test of single-edge cracked membranes under a long duration. (a) Stress-stretch curves. (b and c) Photographs of the pre-cracked sample at different cycles. (b) Under a stretch amplitude of 1.20, no crack growth on the membrane was observed after 1,000,000 cycles. (c) Under a stretch amplitude of 1.40, the sample necked after 1,200 cycles, but no crack growth was observed after 1,500,000. Markers in (b) and (c) indicate the slippage of samples is negligible in the fatigue test.

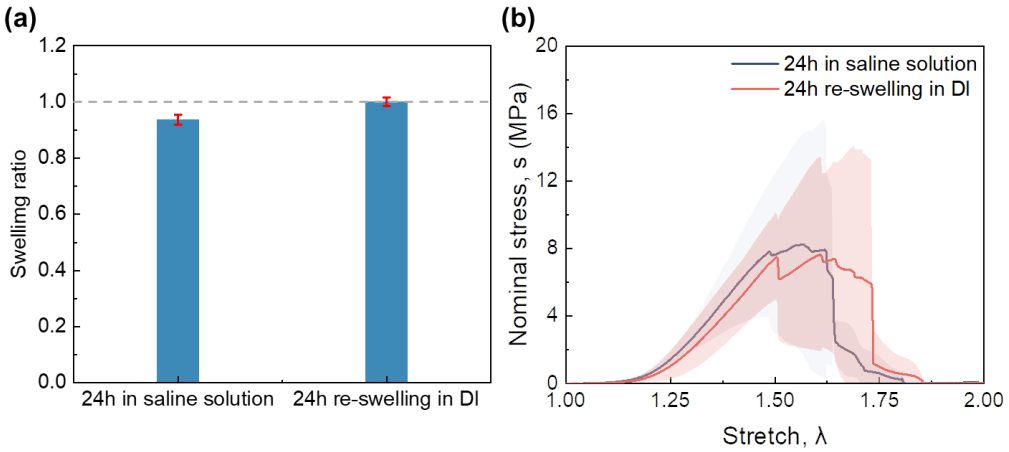

Fig. S15 Evaluating the influence of aqueous environment on the mechanical response of fixed membrane. (a) Swelling ratio of samples after immersed in saline solution and deionized (DI) water. (b) Stress-stretch curves of samples immersed in saline solution and re-swelling in DI water. Solid lines and shadow bands are mean values and standard deviation, n = 3 in each group.